Size effect on branched sideways cracks in orthotropic fiber composites

Abdullah Dönmez & Zdeněk P. Bažant

International Journal of Fracture

ISSN 0376-9429
Volume 222
Combined 1-2

Int J Fract (2020) 222:155-169
DOI 10.1007/s10704-020-00439-1

Springer

Int J Fract (2020) 222:155–169
https://doi.org/10.1007/s10704-020-00439-1

ORIGINAL PAPER

Size effect on branched sideways cracks in orthotropic fiber composites

Abdullah Dönmez · Zdeněk P. Bažant

Received: 30 August 2019 / Accepted: 7 February 2020 / Published online: 22 February 2020

Abstract In edge-notched tension specimens of unidirectional fiber-polymer composites, an initial transverse crack or notch might not propagate forward. Instead, sideways cracks parallel to fibers may grow axially from the initial crack tip. When the fibers are inclined from the specimen axis, a sideways crack propagates along the inclined fibers. Unless a potential sideways orthogonal cohesive crack is considered to exist a priori at the right location, the cohesive crack model cannot predict the sideways branching correctly. The crack band model can, because it involves a damage model with tensorial strength criterion, instead of scalar stress-separation law. We obtain approximate analytical solutions by the method of stress relief zones bordered by lines of slope k calibrated by J-integral. Our analysis, verified by finite element simulations, yields formulae for the structure size effect of orthogonal or inclined sideways cracks, taking into account the effect of the length of original transverse crack or notch, and the effect of the ratio of fracture energies Γ_f and Γ_s of the forward and sideways cracks, respectively. The sideways cracks develop only if the ratio Γ_s/Γ_f is small enough, below a certain critical value (on-the-order of 10^{-1}) depending on material parameters. Measuring the size effect of sideways cracks yields Γ_s and the corresponding fracture process zone size. The theory is shown to match Nairn's tests with varying notch depths. The results can be applied to all kinds of orthotropic composites.

Keywords Crack branching · Quasibrittle fracture mechanics · Crack band model · Cohesive crack model · Strength scaling · Fracture energy · Fracture process zone · Unidirectional fiber composites · Laminates · Crack stability

1 Introduction

In edge-notched tensile strip specimens of highly orthotropic fiber composites, such as unidirectional prepregs or laminates of a two-directional orthotropic layup with weak transverse fibers, the crack often does not grow along the notch direction. Rather, a sideways crack branched in the direction of tension and normal to the notch direction may typically develop (Fig. 1). Similar behavior is known for wood.

Observations of the branched sideways cracks in experiments have often been invoked to claim that fracture mechanics is not applicable to fiber composites. It is, of course, true that the linear elastic fracture mechanics (LEFM) does not apply. It is also true that the cohesive crack model (Barenblatt 1962; Hillerborg et al.

A. Dönmez
Ístanbul Teknik Üniversitesi, Istanbul, Turkey
e-mail: donmezab@itu.edu.tr

A. Dönmez
Northwestern University, Evanston, USA

Z. P. Bažant (✉)
Civil and Mechanical Engineering and Materials Science, Northwestern University, Evanston, USA
e-mail: z-bazant@northwestern.edu

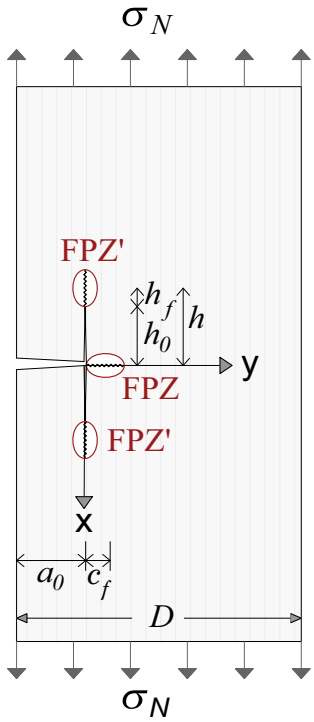

Fig. 1 General sideways crack propagation

1976), being a line crack model with a scalar relation between stress and crack opening, cannot predict sideways crack branching, unless a potential sideways cohesive crack zone is postulated to exist a priori at the right place where branching is suspected, as done by (Noselli et al. 2013; Tankasala et al. 2017, 2018). However, this is not a general prediction model.

Predicting the germination of a sideways crack from the fracture process zone (FPZ) requires quasibrittle fracture mechanics. Unlike the cohesive crack model, it takes into account the tensorial damage in the FPZ at the crack front. Its simplest form, to be used here, is the crack band model. Originated in the 1980s (Bažant 1982, 1984; Bažant and Oh 1983; Bažant and Planas 1997), it is distinct from, and more general than, the cohesive crack model. That model cannot capture the tensorial strength limits and damage in the FPZ. Neither can it capture the huge effect of crack-parallel compression, the axial splitting fracture under uniform compression, the transition from distributed cracking to a localized crack, and the tensorial behavior of FPZ under nonproportional or fatigue loading. Neither can these features be captured by the phase-field model (Ming-Yuan and Hutchinson 1989; Parmigiani and Thouless 2006; Martnez and Gupta 1994; Suo et al. 1991), as it now exists. Yet they can by the crack band model.

The basic idea of the crack band model (Bažant and Oh 1983; Bažant and Planas 1997; Bažant and Le 2017) for strain-softening in tension as well as shear is to avoid spurious mesh-sensitivity by adjusting the material parameters that control the steepness of the softening post-peak stress–strain relation and describe smeared cracking. In this way, the energy dissipated by fracture per unit length of the crack band (and per unit out-of-plane thickness) is made approximately independent of the element size. The adjustment of material parameters depending on element size also circumvents the problems of unlimited strain localization and of ill-conditioning associated with partial differential equations for the strain-softening continuum. The crack band offers a simple way to capture the deterministic (or energetic) size effect (Bažant and Oh 1983; Bažant and Planas 1997).

The simplest way to use the crack band model is to use an element size, h, such that a sudden (or vertical) stress drop from the peak-stress point (or generally from the limit point at which the tangential stiffness matrix becomes singular) would dissipate an energy equal to the fracture energy of the material. If h is kept the same for various structure sizes, no adjustment of post-peak softening slope is needed, which is what is done here (Bažant and Oh 1983; Bažant and Planas 1997). Such a fixed element size may then be regarded as the material characteristic length, $h = l_0$ (akin to Irwin's length, l_0, in cohesive fracture mechanics).

Early studies of sideways crack branching, aka kinking, used criteria based on the near-tip stress field, which cannot capture the energetic (non-statistical) size effect. The first such study apparently belongs to Cook et al. (1964), who assumed the existence of a weak plane orthogonal to the notch. This approach was later refined in (Goree and Gross 1980; Buczek and Herakovich 1985; Gupta et al. 1992). An explicit solution of the stress field near the crack tip in a unidirectional composite was given by Sih et al. (1965). They also studied energy-based criteria and proposed for fiber composites a criterion based on a critical strain energy density, which, however, was not generally accepted.

The power of the crack band model for predicting sideways cracks was recognized by (Pineda and Waas 2013; Xu et al. 2015; Xu and Waas 2016), who exploited the tensorial nature of the stress and strain within the band to predict orthogonal sideways cracks

in fiber polymer composites. Here we aim to use the crack band model to extend Waas et al.'s work to the problem of scaling and derive closed formulae for the size effect.

The size effect is a quintessential property of fracture mechanics. It is particularly important for quasibrittle fracture, and cannot be captured by strength criteria alone. The existence of size effect is one proof that the failure of composites cannot be predicted from stress or strain criteria alone, which predict no size effect, yet are still widely encountered in practice. It is still widely believed that the size effects observed in fiber composites are solely Weibullian. But this is erroneous and can be gravely misleading. The statistical aspect is only secondary and becomes significant only for very large structures; see (Bažant and Le 2017; Bažant 2019).

2 Orthotropic elastic constants of unidirectional fiber composites predicted from constituent properties

First, we need to formulate the elastic constitutive model. We consider orthotropic fiber laminates with unidirectional fiber reinforcement in the x-direction (Fig. 1), and, up to the material strength limit, we treat the laminate as orthotropic linearly elastic. The two-dimensional orthotropic elastic stress–strain relations are:

$$\begin{aligned}
\sigma_{xx} &= E_{xx}\epsilon_{xx} + E_{xy}\epsilon_{yy}\\
\sigma_{yy} &= E_{xy}\epsilon_{xx} + E_{yy}\epsilon_{yy}\\
\tau_{xy} &= G_{xy}\gamma_{xy}\\
E_{xx} &= \frac{E_1}{1-\nu_{12}\nu_{21}};\quad E_{xy} = \frac{\nu_{21}E_1}{1-\nu_{12}\nu_{21}}\\
E_{yy} &= \frac{E_2}{1-\nu_{12}\nu_{21}};\quad G_{xy} = G_{12}.
\end{aligned} \tag{1}$$

where σ_{xx}, σ_{yy} = normal stresses, τ_{xy} = shear stress, ϵ_{xx}, ϵ_{yy} = normal strains and $\gamma_{xy} = 2\epsilon_{xy}$ = shear angle. Very good estimates are provided by the Hill–Hashin–Christensen–Lo formulae developed in (Hill 1965; Hashin 1965; Christensen and Lo 1979; Huang et al. 2011).

$$\begin{aligned}
E_1 &= V_f E_f + V_m E_m + \frac{4(\nu_f-\nu_m)^2 V_f(1-V_f)}{\frac{V_f}{k_m}\frac{1-V_f}{k_f}\frac{1}{G_m}}\\
E_2 &= \frac{2}{\frac{0.5}{K_L}+\frac{0.5}{G_{23}}+\frac{2\nu_{12}^2}{E_1}}\\
G_{xy} &= G_m\frac{G_f+G_m+V_f(G_f-G_m)}{G_f+G_m-V_f(G_f-G_m)}\\
\nu_{12} &= V_f\nu_f + V_m\nu_m\\
&\quad + \frac{(\nu_f-\nu_m)V_f(1-V_f)}{\frac{V_f}{k_m}+\frac{1-V_f}{k_f}+\frac{1}{G_{12}}}\left(\frac{1}{k_m}-\frac{1}{k_f}\right)\\
K_L &= \frac{3k_m+G_m}{3} + \frac{V_f}{\frac{1}{k_f-k_m+\frac{G_f-G_m}{3}}+\frac{1-V_f}{k_m+\frac{4G_m}{3}}}\\
G_{23} &= G_m\left(1+\frac{V_f}{\frac{G_m}{G_f-G_m}+\frac{(k_m+7G_m/3)(1-V_f)}{2k_m+8G_m/3}}\right)\\
k_f &= \frac{E_f}{3(1-2\nu_f)};\quad k_m = \frac{E_m}{3(1-2\nu_m)}
\end{aligned} \tag{2}$$

where V generally refers to volume fraction, E to modulus of elasticity, ν to Poisson's ratio and G to shear modulus, and subscripts f and m refer to the fibers and matrix.

The preliminary analysis used Bažant's 1968 simpler approximation (Bažant 1968; Bažant and Cedolin 2010) based on a mixture of parallel and series couplings. It gave similar results even though the estimate of E_{yy} has a significant error (almost 50% in some cases).

3 Simple approximate analysis based on idealized energy release zones

3.1 Method of "stress relief zones" bordered by "stress diffusion" lines of slope calibrated by J-integral

Consider an elongated rectangular strip with a transverse notch of length a_0, as shown in Fig. 2a. Uniform uniaxial tension, σ_N, is applied at remote ends. Reinforcing fibers in the longitudinal direction, and nonexistent (or weak) in the transverse direction, cause the fracture energy Γ_f for forward (i.e., transverse) crack propagation to be much larger than the fracture energy Γ_s for the longitudinal crack propagation (orthogonal to the notch); i.e., $\Gamma_f \gg \Gamma_s$. Obviously,

Γ_s represents a shear fracture energy predominantly, because the vertical plane emanating from the notch tip (Fig. 2b) is subjected to shear stress, due to different longitudinal strains caused by longitudinal contraction of the unloaded material on the left of that crack.

We will now use the simple method of "stress relief" zones bordered by "stress diffusion" lines. In this method, which met with success in some other fracture problems (Bažant 1984; Bažant and Planas 1997, e.g), we assume the stress σ in the cross-hatched triangular zone limited by a line of slope $1/k$, emanating from the center of the FPZ at the notch or crack tip (Fig. 2), to get reduced to zero, and the stress outside this zone to remain unaffected by the notch or crack. At first, this method may look too crude, because in reality the stress field varies gradually, and the stress concentration near the crack front is ignored.

It has nevertheless been shown that this method leads to the correct general form of the equation relating the load, fracture-caused displacement, and structure size D. To make not only the form but also the equation coefficients exact, the slope k must be determined either by matching the energy release rate based on k to the J-integral calculated by FE or by a comparison with other features of a full elasticity solution, if available.

The useful feature of this method is that, for geometrically scaled structures, (1) the optimal slope k is exactly the same for LEFM and almost the same for nonlinear fracture models, and that (2) the stress relief zones consist of two parts, one of which, representing the unloaded undamaged material, scales with D quadratically, and another, corresponding to the damaged FPZ, scales with D linearly; i.e., $\mathcal{G} \propto D^2$ or D. The combined scaling can thus give the correct form of quasibrittle size effect, which is transitional between ductility and brittleness. It was via the stress relief zones that Bažant's size effect law (SEL) for concrete and other quasibrittle materials was originally derived in 1984 (Bažant 1984). The resulting equation form of SEL was later validated in several other ways, e.g., by asymptotic matching combined with equivalent LEFM and J-integral analysis (Bažant and Planas 1997; Bažant and Le 2017; Bažant and Kazemi 1990; Bažant 1997, 2005). Recently, the same method was successfully used for reinforced concrete shear walls (Rasoolinejad and Bažant 2019).

3.2 Forward crack propagation

For fracture analysis, we need the density of complementary energy of unidirectional composite subjected to uniform uniaxial stress $\sigma_{xx} = \sigma_N$ along the fibers. Inverting the stress–strain relations in Eqs. (1) with (2), we get the material compliance matrix and particularly the effective elastic modulus $\hat{E}$ for uniaxial stress along fibers. This yields the longitudinal strain $\epsilon_{xx} = \sigma_{xx}/\hat{E}$ and the complementary energy density

$$\bar{\Pi}^* = \sigma_N^2/2\hat{E}, \quad \hat{E} = E_{xx} - E_{xy}^2/E_{yy} \tag{3}$$

Denote now as c_f the half-length of the FPZ in the sense of equivalent linear elastic fracture mechanics (LEFM); c_f is approximately equal to $\frac{1}{3}$ to $\frac{1}{2}$ of the FPZ length, and is approximately a material constant [c_f can be precisely identified through the size effect analysis of geometrically scaled specimens; see Fig. 2 and (Bažant and Yu 2011; Cusatis and Schauffert 2009)].

Let $a = a_0 + c_f$ = total length of the equivalent LEFM crack. The complementary strain energy is assumed to be released from two symmetric triangular stress-relief zones bounded by certain slopes k (shaded in Fig. 2b);

$$\Pi^* = b\,\frac{\sigma_N^2}{2\hat{E}}\,2\,\frac{a\cdot ka}{2} \tag{4}$$

where b is the thickness of the laminate plate. So, the energy release rate of the forward crack (transverse to the fibers), which must be during propagation equal to the fracture energy, Γ_f, for transverse fracture, is

$$\mathcal{G} = \frac{1}{b}\frac{\partial \Pi^*}{\partial a} = \frac{\sigma_N^2}{2\hat{E}}\,2\,k(a_0 + c_f) = \Gamma_f \tag{5}$$

From this, for transverse crack propagation,

$$\sigma_N = \sqrt{\frac{\hat{E}\Gamma_f}{k(a_0 + c_f)}} = \frac{\sigma_0}{\sqrt{1 + D/D_0}} \tag{6}$$

$$\text{where} \quad D_0 = c_f(D/a_0), \quad \sigma_0 = \sqrt{\hat{E}\Gamma_f/c_f k}. \tag{7}$$

where $D_0 = c_f(D/a_0)$ is a constant for geometrically scaled structures of different sizes, for which the notch lengths must also be similar, i.e, a_0/D is the constant. Note that Eq. (6) has the exact form of Bažant's SEL (Bažant 1984; Bažant and Kazemi 1990), although parameters k (depending on structure shape) and material constant c_f must be determined separately. This law has been rigorously derived by asymptotic matching based on equivalent LEFM, or on J-integral (Bažant and Planas 1997; Bažant 1997, 2005).

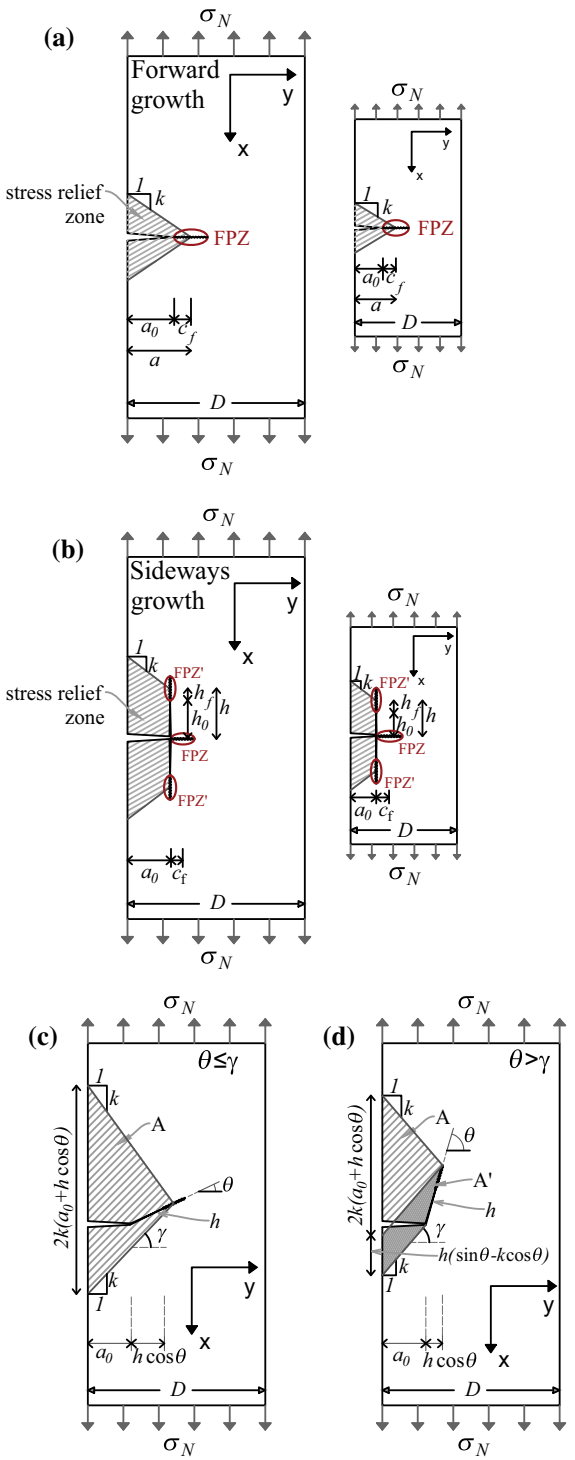

Fig. 2 Crack propagation in **a** forward, **b** sideways for scaled structures and **c**, **d** inclined directions

What is particularly useful in this simple approach is that, once the correct k-value for a given specimen geometry is identified and a realistic c_f is known, one can easily obtain the correct scaling, particularly the quasibrittle deterministic (or energetic) size effect, giving the transition from quasi-ductile failure to brittle failure. To get a general FE solution, one would have to supplement it by asymptotic matching, which would be much more tedious. Any accurate analytical solution of the boundary value problem would be possible only for $c_f = 0$, i.e., for LEFM, emulating the approach in Suo et al. (1991).

3.3 Propagation of orthogonal sideways cracks

Let us now analyze orthogonally branched sideways cracks propagating in the direction of axis x. The origin of coordinates (x, y) is placed at the tip of the notch or preexisting crack (Fig. 2b). The notch in y-direction (transverse to fibers) causes the material to unload in the vicinity of the notch on the left of axis x but not in the region on the right of that axis. So the material to the left of x contracts in x direction, while to the right x it does not. It is thus intuitively clear that shear stresses τ_{yx} must develop along axis x. A normal stress across that axis must develop as well. This is what intuitively explains, along with the material weakness along axis x, the propagation of sideways crack parallel to the applied tension.

The energy release rate at constant load σ_N does not increase as the sideways crack grows, as confirmed by what follows. Neither it decreases. This means that the propagation of branched sideways crack is at the limit of stability, and so these cracks can grow simultaneously in opposite directions (i.e., both up and down in Fig. 2b). Experiments (Nairn 1988a; Newaz 1985; Lee and Pharr 2019) confirm it.

We consider a longitudinal crack emanating from the transverse crack tip (Fig. 2b); h_0, h = its lengths up to the beginning of its FPZ and up to the approximate half-length of the FPZ (making h the length of an equivalent LEFM crack); $h_f = h - h_0$ is roughly the half-length of the FPZ, treated approximately as a constant.

The total release of the complementary strain energy from the cross-hatched stress-relief zone in Fig. 2b, consisting of one triangle and one rectangle, is

$$\Pi^* = b\,\frac{\sigma_{Ns}^2}{2\hat{E}}\,2\left(a_0 h + \frac{a_0 \cdot a_0 k}{2}\right) \tag{8}$$

where $h = h_0 + h_f$. The rate of energy release from one longitudinal sideways crack, which must be equal to the fracture energy, Γ_s, for sideways crack propagation, must be equal to effective fracture energy Γ_s for the sideways cracks

$$\mathcal{G} = \frac{1}{b}\left[\frac{\partial \Pi^*}{\partial h}\right]_P = \frac{\sigma_{Ns}^2}{2\hat{E}}\, a_0 \;=\; \Gamma_s \tag{9}$$

Γ_s is fracture energy of sideways crack, which is here assumed to be approximately a constant. The crack is not of pure mode II, but is mixed with a mode I component because non-negligible normal stresses develop on the crack (this is captured automatically if the fracture front is described tensorially, as in the crack band model). The nominal strength of structure with a sideways crack then is

$$\sigma_{Ns} = \sqrt{\frac{2\hat{E}\Gamma_s}{a_0}} \tag{10}$$

Note that this result is independent of h and h_f, i.e., of the length of the sideways crack and of its FPZ length. This means that, after reaching the maximum load, there load evolution must exhibit a quasi-plastic plateau, instead of gradual softening which is endemic for forward propagation. However, as seen in Eq. (10), there is a size effect of initial relative cracks length, α_0. For geometric similarity, i.e., for $a_0 \propto D^{-1/2}$, this size effect is of the LEFM type, $\sigma_{Ns} \propto (\text{size})^{-1/2}$, which is the strongest possible.

When the load is gradually increased, the sideways crack will start growing at the first opportunity it has. It will grow when

$$\sigma_{Ns} \le \sigma_N \quad \text{or} \quad \frac{2\hat{E}\Gamma_s}{a_0} = \frac{\hat{E}\Gamma_f}{k(a_0 + c_f)} \tag{11}$$

$$\text{or} \quad \boxed{\frac{\Gamma_s}{\Gamma_f} = \frac{a_0}{2k(a_0 + c_f)}} \tag{12}$$

If, in Eq. (12), the left-hand side > the right-hand side, the sideways fracture cannot grow, and if <, the energy released by growth exceeds the energy dissipated at the front of sideways fracture, the sideways crack will grow dynamically.

Since $c_f \ge 0$, the last equation lets us state a weak criterion that is necessary, though not sufficient, for sideways crack growth to happen:

$$\boxed{\Gamma_s < \Gamma_f/2k} \tag{13}$$

Solving Eq. (12) for a_0 further reveals the existence of a critical length a_0 of transverse notch or crack below which the sideways crack cannot form:

$$a_{0cr} = \frac{c_f}{\Gamma_f/2k\Gamma_s - 1} \tag{14}$$

Rather, a short forward crack will grow first, and then a sideways crack will start once a_{0cr} is reached, provided that Γ_s is small enough, such that $\Gamma_s < \Gamma_f/2k$. In view of inequalities (11) and (12), we thus have the limits:

$$\lim_{\Gamma_s/\Gamma_f \to k/2} a_{0cr} = \infty \tag{15}$$

$$\lim_{\Gamma_s/\Gamma_f \to \infty} a_{0cr} = 0 \tag{16}$$

It is interesting to check the size effect on nominal strength when the specimen is scaled up geometrically, i.e., when a_0/D is kept constant, D being the specimen size. From Eq. (12),

$$\boxed{\sigma_{Ns} = \sqrt{C/D}} \quad \text{where} \quad C = 2\hat{E}\Gamma_s(D/a_0) = \text{constant} \tag{17}$$

So the crack lengths h and h_0 are irrelevant and the sideways cracks exhibit the LEFM scaling even if the FPZ size, h_f, is finite. This simplifies the testing of Γ_s but prevents the use size effect testing to measure h_f for the orthogonal sideways cracks. Note also that the size effect on the sideways crack is stronger than it is on the forward crack, becoming identical only in the limit of infinite size.

To determine Γ_s, one may test the strength, or σ_N, of specimens of different sizes D. Keeping the same notch ratio a_0/D (and the same length-to-width ratio of the specimen) would make the calculations simpler. Because of scatter, test repetition is necessary. Unlike the testing of Γ_f and c_f (Bažant and Kazemi 1990; Bažant et al. 1996), two-dimensional regression is unnecessary. It is a simple single variable statistics because the FPZ size, h_f, need not be known. For each measured σ_{Ns}, one can use Eq. (17) to calculate the values of:

$$\Gamma_s = \frac{\sigma_{Ns}^2 D}{2\hat{E}(D/a_0)} \tag{18}$$

From the collection of measured Γ_s-values, one gets their mean and standard deviation. It is of course possible to test specimens with sufficiently different a_0 values and dissimilar sizes D. But, according to the experi-

ence with concrete (Bažant and Planas 1997), one must expect a more scattered collection of measured Γ_s values, especially because the present approach based on energy release zones becomes less accurate when the specimen shapes are not similar.

3.4 Non-orthogonal sideways crack propagation along inclined fibers

Consider now a single-edge-notched tension (SENT) specimen in which the fibers deviate from the longitudinal direction by either 45° or −45°. Let x be the fiber direction y normal to it. For a uniaxial tensile stress σ_N applied in the longitudinal direction, the Mohr circle readily gives, in coordinates x and y, the stresses are $\sigma_{xx} = \sigma_{yy} = \sigma_{xy} = \sigma_N/2$. Inverting Eqs. (1) gives:

$$\epsilon_{xx} = \frac{E_{yy} - E_{xy}}{E_{xx}E_{yy} - E_{xy}^2}\,\frac{\sigma_N}{2}$$
$$\epsilon_{yy} = \frac{E_{xx} - E_{xy}}{E_{xx}E_{yy} - E_{xy}^2}\,\frac{\sigma_N}{2} \tag{19}$$

The complementary strain energy density is then calculated as

$$\bar{\Pi}^* = \frac{1}{2}(\sigma_{xx}\epsilon_{xx} + \sigma_{yy}\epsilon_{yy} + \sigma_{xy}\gamma_{xy}) = \frac{1}{2}(\epsilon_{xx} + \epsilon_{yy} + \gamma_{xy})\,\frac{\sigma_N}{2} = \frac{\sigma_N^2}{2E_{45}}, \tag{20}$$

$$\frac{1}{E_{45}} = \frac{1}{4}\left(\frac{E_{xx} + E_{yy} - 2E_{xy}}{E_{xx}E_{yy} - E_{xy}^2} + \frac{1}{G_{xy}}\right) \tag{21}$$

Next consider a bi-directional composite in which one half of the fibers run in direction x and one half in direction y. The strains, taken separately for each inclination, are equal, including γ_{xy}. The stresses, which are equal for both inclinations, are summed. But the stresses for both cases are equal, too.

Therefore, the foregoing equations for stresses and complementary energy remain valid. The only difference, which is irrelevant for the present analysis, is that the specimen cross sections remain normal to the longitudinal axis while, in the case of fibers inclined in only one direction, the shear strain causes the cross sections to rotate.

More generally, the unidirectional fibers in the notched specimen can run at any angle θ with the notch. We will not bother to set up the equations for the stresses, but it is obvious that $\hat{E}$ is a certain effective modulus depending on angle θ. When the fiber direction forms a skew angle θ with the notch or existing crack (Fig. 2c), the crack propagates in that sideways direction, too. Here one might think of two options: (1) Two inclined cracks propagating symmetrically on both sides of the notch, or (2) only one inclined propagating on one side of the notch. Calculations showed, however, that the former option is unstable under load control, because, unlike the orthogonal sideways cracks, the equilibrium propagation of inclined cracks would require a decreasing load. So we consider an inclined crack on one side only, as shown in Fig. 2c, d, and consider that the maximum load occurs as soon as the FPZ forms, i.e., for $h = h_f$, with $h_0 = 0$.

Denote $\gamma = \arctan k$ = angle of stress diffusion line with the notch, and θ = angle of the fibers and the sideways crack with the notch. For simplicity, we consider the stress relief zones on both sides of the notch to be bordered by the same slope k, as shown in Fig. 2c, d. Actually, on the side opposite to inclined crack one might expect a different slope k', but there is no way to determine it in a simple way since, from the equivalence with J-integral, we can identify only one slope.

The energy release areas are A and A', respectively, as marked and shaded in Fig. 2c, d. For both cases the total area, A_T, may be written as

$$A_T = A + A', \quad A = k(a_0 + h\cos\theta)^2$$
$$A' = \langle \sin\theta - k\cos\theta \rangle \left(\frac{1}{2}h^2\cos\theta + ha_0\right) \tag{22}$$

where $\langle x \rangle = \max(x, 0)$ = positive part of the argument = Macauley brackets (so A' vanishes when $\theta < \gamma$). The complementary energy density driving the fracture is assumed to be $\sigma_N^2/2\hat{E}$ where $\hat{E}$ is a certain effective elastic modulus (depending on fiber content and fiber orientation). For the case of $\theta = 45°$, $\hat{E}$ is equal to E_{45} in Eq. (21). The estimate of complementary energy released by fracture is $\Pi^* = bA_T(\sigma_N^2/2\hat{E})$. Then, introducing dimensionless crack length parameters,

$$h = \eta D, \quad h_0 = \eta_0 D, \quad a_0 = \alpha_0 D \tag{23}$$

we obtain the energy release rate of the branched sideways crack in the form:

$$\mathcal{G} = \frac{1}{b}\frac{\partial \Pi^*}{\partial h} = \frac{\sigma_N^2}{2\hat{E}} D\tilde{g}(\eta,\alpha_0)\tilde{g}(\eta,\alpha_0)$$
$$= (\alpha_0 + \eta\cos\theta)(2k\cos\theta + \langle \sin\theta - k\cos\theta\rangle) \quad (24)$$

It may be checked that Eqs. (5) and (9) are the limiting cases for $\theta = 0$ and $\theta = \pi/2$. For the non-orthogonal fibers and crack, it is found that the energy release rate at constant load, or $\tilde{g}(\eta,\alpha_0)$, is increasing with crack length h (which is the case of positive geometry). This means that the maximum load is reached as soon as the sideways FPZ of length h_f is formed ($h = h_f$). After that moment, there is postpeak softening and the non-orthogonal sideways crack grows dynamically.

In Eq. (24), we may now approximate function $\tilde{g}(\eta,\alpha_0)$ by the first two terms of Taylor series expansion with respect to η at constant α_0 and θ:

$$\tilde{g}(\eta,\alpha_0) = \tilde{g}_0(\alpha_0) + \tilde{g}_0'(\alpha_0)h_f/D \quad (25)$$

where h_f, the half-size of the FPZ, is assumed to be approximately constant when size D is scaled. Next we may set $\mathcal{G} = \Gamma_s'$ and, considering scaled geometrically similar structures with similar cracks, for which η, η_0, α_0 are constant, we obtain

$$\sigma_N = \sqrt{\frac{\hat{E}\Gamma_s'}{D[\tilde{g}(\alpha_0) + \tilde{g}'(\alpha_0)h_f/D]}} = \frac{\sigma_0}{\sqrt{1 + D/D_0}} \quad (26)$$

$$\text{where} \quad D_0 = h_f\frac{\tilde{g}'(\alpha_0)}{\tilde{g}(\alpha_0)}, \quad \sigma_0 = \sqrt{\frac{\hat{E}\Gamma_s'}{\tilde{g}'(\alpha_0)}}. \quad (27)$$

4 Material strength limits for FE analysis with crack band model

The cohesive crack model, which is a line crack model with a one-dimensional stress–strain law, requires one strength limit, the tensile strength. Generalized to mixed mode, it requires a potential depending on two scalar variables, the normal and tangential displacements. But for FE fracture analysis with the crack band model, we need a triaxial tensorial strength criterion for the material in the FPZ.

In the crack band model, infinitely many microcracks of infinitely small openings are imagined to be continuously distributed (or smeared) over the finite element. This can be conveniently modeled by reducing the material stiffness and strength in the direction normal to the crack band after the peak strength of the material has been reached. Such changes of the stiffness matrix are relatively easy to implement in a FE code, and, hence, the appeal of smeared cracking. The evolution of the cracking process down to zero stress at full fracture implies strain softening, i.e., a postpeak gradual decline of stress at increasing strain. So, according to the crack band concept, using a post-peak softening law, or defining a characteristic length, or keeping the same element size in the damage or failure zones, are all equivalent.

Matzenmiller et al. (1995) used a continuum damage mechanics coupled with failure criteria for the anisotropic materials. This method is adopted here, and the damage tensor $\boldsymbol{Q}$ is used for the transition between the undamaged and damaged material. For plane stress conditions, this transition is addressed as follows:

$$\hat{\boldsymbol{\sigma}} = \boldsymbol{Q}\boldsymbol{\sigma} \quad (28a)$$

$$\boldsymbol{Q} = \begin{bmatrix} \frac{1}{q_{11}} & 0 & 0 \\ 0 & \frac{1}{q_{22}} & 0 \\ 0 & 0 & \frac{1}{q_{12}} \end{bmatrix}; \hat{\boldsymbol{\sigma}} = \begin{bmatrix} \hat{\sigma}_x \\ \hat{\sigma}_y \\ \hat{\tau}_{xy} \end{bmatrix}; \boldsymbol{\sigma} = \begin{bmatrix} \sigma_x \\ \sigma_y \\ \tau_{xy} \end{bmatrix} \quad (28b)$$

where $\hat{\boldsymbol{\sigma}}$ and $\boldsymbol{\sigma}$ correspond to the stress vectors for damaged and undamaged material respectively. The damage variables q_{11}, q_{22} and q_{12} are the functions of the strain values. The threshold values for the strains can be found by using the Hashin's criteria: (Hashin 1980)

$$\text{for } \sigma_x > 0: \quad \frac{\varepsilon_x}{e_{ft}} < 1 \quad (29a)$$

$$\text{for } \sigma_x < 0: \quad \left|\frac{\varepsilon_x}{e_{mc}}\right| < 1 \quad (29b)$$

$$\text{for } \sigma_y > 0: \quad \left(\frac{\gamma_{xy}}{\gamma_m}\right)^2 + \left(\frac{\varepsilon_y}{e_{mt}}\right)^2 < 1 \quad (29c)$$

$$\text{for } \sigma_y < 0: \quad \left(\frac{\gamma_{xy}}{\gamma_m}\right)^2 + \left(\frac{\varepsilon_y}{e_{mc}}\right)^2 < 1 \quad (29d)$$

where $e_{ft}, e_{mc}, e_{mt}, \gamma_m$ refer to tensile strain threshold of the fibers and to the limit values of compressive, tensile and shear strains of the matrix, respectively. These thresholds correspond to f_{ft}, f_{mc}, f_{mt}, and τ_m in terms of stress quantities. Note that Eq. (29a) depends on only the fiber strength while Eqs. (29b, 29c, 29d) are independent of the fiber parameters.

The damage variables q_{11}, q_{22} and q_{12} can be calculated as in Eq. (30).

$$\text{for } \sigma_x > 0: \quad q_{11} = \exp\left(-c_f \langle \frac{\varepsilon_x}{e_{ft}} - 1 \rangle\right) \tag{30a}$$

$$\text{for } \sigma_x < 0: \quad q_{11} = \exp\left(-c_m \langle \left|\frac{\varepsilon_x}{e_{mc}}\right| - 1 \rangle\right) \tag{30b}$$

$$\text{for } \sigma_y > 0: \quad q_{22} = \exp\left(-c_m \langle c_{sy} \left(\frac{\gamma_{xy}}{\gamma_m}\right)^2 + \left(\frac{\varepsilon_y}{e_{mt}}\right)^2 - 1 \rangle\right) \tag{30c}$$

$$q_{12} = \exp\left(-c_m \langle \left(\frac{\gamma_{xy}}{\gamma_m}\right)^2 + \left(\frac{\varepsilon_y}{e_{mt}}\right)^2 - 1 \rangle\right) \tag{30d}$$

$$\text{for } \sigma_y \langle 0: \quad q_{22} = \exp\left(-c_m \langle c_{sy} \left(\frac{\gamma_{xy}}{\gamma_m}\right)^2 + \left(\frac{\varepsilon_y}{e_{mc}}\right)^2 - 1 \rangle\right) \tag{30e}$$

$$q_{12} = \exp\left(-c_m \langle \left(\frac{\gamma_{xy}}{\gamma_m}\right)^2 - c_{ys} \left(\frac{\varepsilon_y}{e_{mc}}\right)^2 - 1 \rangle\right) \tag{30f}$$

where c_f, c_m, c_{sy} and c_{ys} are the parameters associated with the softening behavior of fiber failure in tension, matrix compression failure, coupling of shear with matrix tensile failure, and coupling of matrix tension with shear failure, respectively. In constructing the damage variables in Eqs. (30), the following assumptions are adopted:

- In compression, the fiber kinking is ignored. Hence, only the matrix strength governs compression failure in the fiber direction.
- The failure in the y-direction (transverse to fiber, weak direction) is controlled only by the matrix. The coupling between the the shear and tension actions is characterized by parameter c_{sy} in Eq. (30c, 30e).
- For the shear damage variable, q_{12}, the positive effect of compressive stresses on the shear failure is taken into account by $-c_{ys}$.
- Since the rupture of fibers is much more brittle than the matrix failure, c_f is taken as 10-times greater than c_m. The coupling of shear to tension or compression failures of the composite is assumed to be 10-times weaker than the coupling of compression or tension failures of the matrix to the shear failure.

After each violation of the strength criterion in Eq. (29), the elastic constants, for that element only, are recalculated according to the Eq. (31);

$$E_{xx} = \frac{q_{11}E_1}{1 - q_{11}q_{22}\nu_{12}\nu_{21}}; \quad E_{yy} = \frac{q_{22}E_2}{1 - q_{11}q_{22}\nu_{12}\nu_{21}}$$
$$E_{xy} = \frac{q_{11}q_{22}\nu_{21}E_1}{1 - q_{11}q_{22}\nu_{12}\nu_{21}}; \quad G_{xy} = q_{12}G_{12} \tag{31}$$

For a simplified analysis, we consider large numbers of c_m and c_f corresponding to a near-vertical drop in the stress–strain response of one finite element. Since the element size, l_0, is fixed so that a vertical stress drop would represent fracture energy of the material, the foregoing strength limits imply the fracture energy for the opening mode of cracks in the forward direction y, i.e.,

$$\Gamma_f = l_0 \frac{f_{yt}^2}{2E_{xx}} \tag{32}$$

The fracture energy of the sideways crack cannot be defined precisely, as a constant. Although the shear failure of this crack is driven mainly by τ_{xy}, it is also influenced σ_y which is nonzero and varies along the crack. As a reasonable approximation, we assume:

$$\Gamma_s = l_0 \max\left(\frac{\tau_m^2}{2G_{xy}}, \frac{f_{mt}^2}{2E_{yy}}\right) \tag{33}$$

Vice versa, if the fracture energies are known (e.g., from size effect tests), the strength limits may be set as

$$f_{yt} = \sqrt{2E_{xx}\Gamma_f/l_0} \tag{34}$$

$$\tau_m = \sqrt{2G_{xy}\Gamma_s/l_0}, \quad f_{mt} = \sqrt{2E_{yy}\Gamma_s/l_0}. \tag{35}$$

5 Verification and calibration by finite element fracture analysis

The foregoing algorithm is implemented in user subroutine VUMAT in commercial FE software (ABAQUS Explicit). Spurious mesh sensitivity and ill-conditioning due to strain-softening are avoided by using the crack band model (Bažant 1984; Bažant and Planas 1997). For best accuracy, the element size is kept constant, the same for every structure size D. The FE mesh consists of linear quadrilateral plane stress elements.

The numerical model for sideways cracking is calibrated by Nairn's (1988a) double-edge notched (DEN) test specimens. Nairn tested 16 UD graphite-epoxy

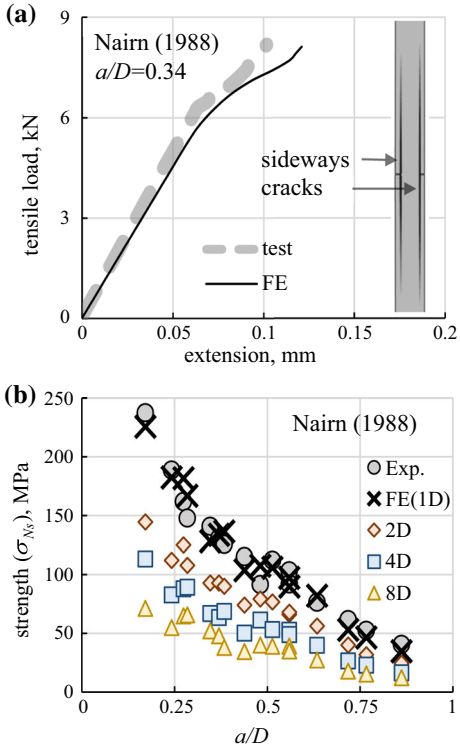

Fig. 3 Sideways crack **a** typical load vs extension curve of a UD fracture specimen, **b** calibration by different initial crack configurations Nairn (1988a)

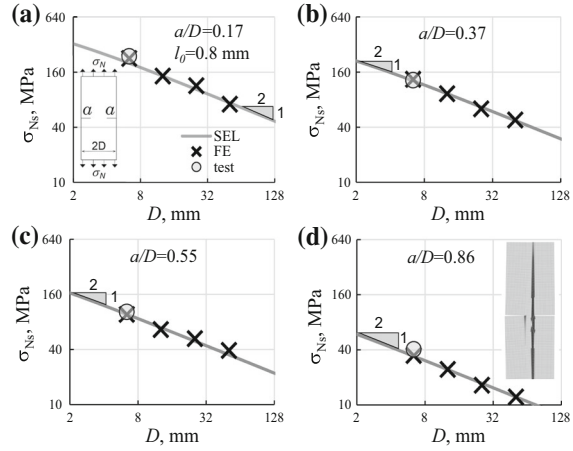

Fig. 4 Size effect predictions of sideway strength for different a/D values. The experimental data points are shown in circles Nairn (1988a)

composite specimens with fiber volume fraction 0.55, having different initial crack length configurations. The material properties are obtained using his test results and Eq. (2). The FE prediction of the orthogonal sideways cracking is shown in Fig. 3a, b.

Since, according to our simplified analysis, the energy release rate for orthogonal sideways crack propagation is constant, the structure is at the limit of stable crack growth. So the cracks could propagate in one or both sideways directions. But computations show a small equilibrium load decrease at the start of sideways cracks, which implies instability for a small crack advance, and causes the sideways crack to grow on only one side, as confirmed by computations. The sideways strength, which may also be called the splitting strength, is defined by the maximum stress at which the sideways crack starts.

Orthogonal sideways crack propagation is simulated for geometrically scaled specimens of four sizes D = 6.35, 12.7, 25.4, 50.8 mm, with relative values D, 2D, 4D, 8D. The calculated nominal strengths are plotted in Fig. 4a–d. The simulations are repeated for each relative transverse notch (or crack) lengths a/D. As seen in the Figs. 3 and 4, σ_{Ns} decreases as the initial (or forward) crack length increases.

FE calculation of the energy release rate $\mathcal{G}$ makes it possible to calibrate the value of the slope k of the energy release zone boundary for the present specimen geometry. Such calculations were made for both the isotropic ($V_f = 0$) and unidirectional transversely isotropic ($V_f = 0.5$) specimens. The $\mathcal{G}$ values were calculated by the J-integrals for forward crack propagation, using FE. The slopes k were then calculated from Eq. (4) and plotted in Fig. 5a. As seen, k is not constant but inreases with the degree of anisotropy and with the relative initial crack length a/D.

The calculated k-values have then been used to determine the critical energy release rates $\mathcal{G}$ for the sideways propagation, Eq. (12). Their comparison is presented, for both isotropic and orthotropic specimens, in Fig. 5b, c. It is not surprising that the critical $\mathcal{G}$ depends on the relative initial crack length a/d (and in general surely also on the structure shape). An increase in a/D leads to a lower critical ratio Γ_s/Γ_f, which implies that the sideways cracks propagate more easily for larger relative initial crack lengths a/D.

It is noteworthy that the energy release rate of sideways propagation of initial crack, computed by FE, is independent of k. This confirms Eq. (9). Hence the k-values cannot be deduced through the fracture energies of sideways crack propagation. The energy release rates

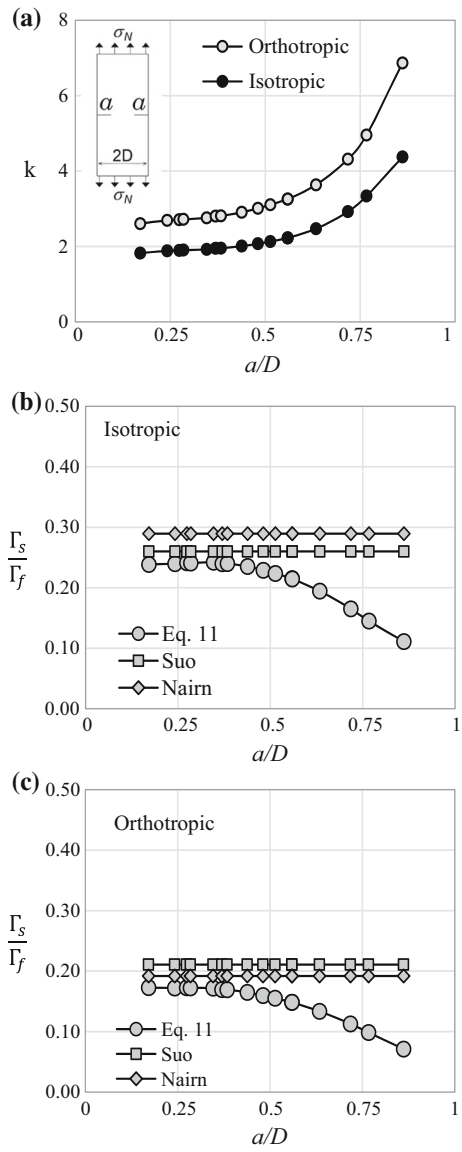

Fig. 5 The variations of **a** the slope of stress diffusion line (k) for both isotropic and orthotropic (UD) cases, and the critical ratio of fracture energies for **b** isotropic, **c** orthotropic cases with respect to dimensionless initial crack length (a/D), [(in comparison with approaches of Suo et al. (1991) and Nairn (1988b)]

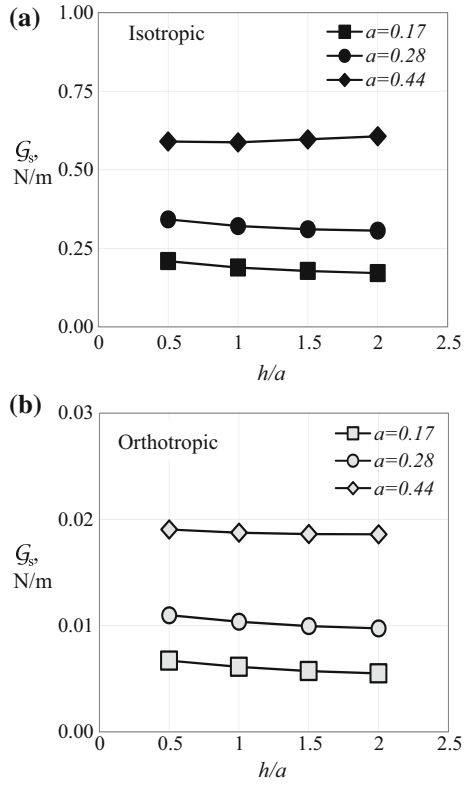

Fig. 6 The variation of energy release rates of sideways cracks propagations for **a** isotropic and **b** orthotropic cases with respect to ratio of h/a for three different initial forward crack length cases

of sideways propagation is also independent of the relative sideways crack length, h/a. To document it, see Fig. 6a, b, showing the J-integral for various values of a/D and h/D values. It is shown that the energy release rates are almost constant as h/a is increased. Moreover, the sideways fracture energy G_s is proportional to the length, a, of the initial forward crack.

The energy released by crack propagation into the tip of an oblique crack depends upon the initial crack length (a), the deflected crack length (h), the inclination angle (θ), and the k values. Keeping a and h constant, we find the energy release to vary with the inclination angle as seen in Fig. 7. Figure 7a shows that the energy release rate increases as the inclination angle becomes smaller. Eq. (24) can then be used to determine the corresponding k values. For the isotropic case, the smallest k is obtained at $\theta = 30°$ (k = 3.85). Figure 7b shows the energy release rate variation for the case of cross-ply fibers oriented at 45°. For this special case, the slope of the stress 'diffusion' lines has its smallest value at $\theta = 45°$ (k = 1.79). Note that the slope of stress diffusion lines (k) becomes smaller for the case of ±45° plies, which is opposite to the case of forward propagation in unidirectional composites (Fig. 5a).

As an example of the proposed FE model, we use the test data by Andersons et al. (2010). We calibrate the model using test data for different ply angles in a

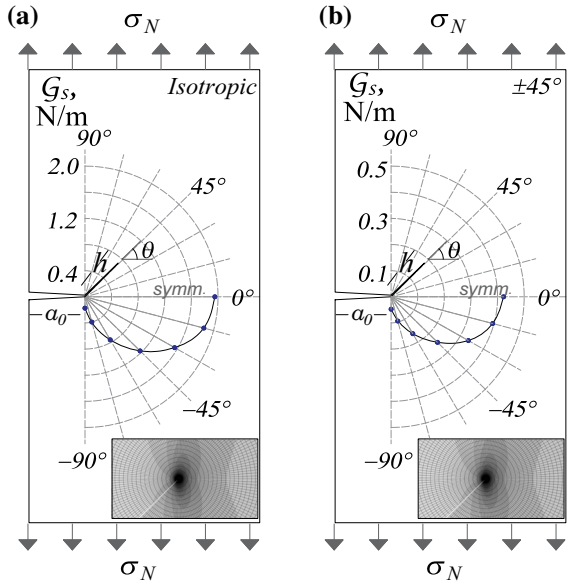

Fig. 7 The variation of energy release rates of inclined crack propagations for **a** isotropic and **b** angle-ply (±45°) cases with respect to inclination angles (θ)

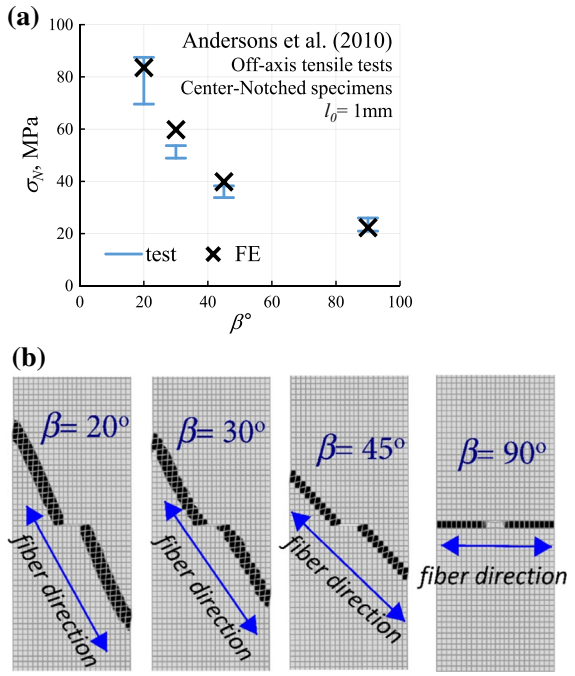

Fig. 8 **a** Off-axis tests of fracture specimen (center edge notched) and **b** corresponding crack propagation according to FE fit (Andersons et al. 2010)

uni-directional glass-epoxy composite under uniaxial tension. The strength values of the center-notched off-axis specimens for various fiber angles are shown in Fig. 8a. The fiber inclination has caused the fracture to emanate from the center notch tips (Fig. 8b).

6 Conclusions

1. While the sideways crack branching in fiber composites, whether orthogonal or inclined, cannot be predicted by the cohesive crack model, it can be by the crack band model—thanks to the damage in the FPZ being modeled as tensorial rather than scalar or vectorial.
2. In unidirectional (UD), as well as strongly orthotropic cross-ply (sCP) composites, the orthogonally branched sideways cracks exhibit a LEFM size effect, i.e., the structural strength is $\propto D^{-1/2}$.
3. The orthogonal sideways cracks (in UD, sCP) grow at constant load and constant energy release rate, and thus are, under load control, at the limit of stable equilibrium, i.e., grow in neutral equilibrium. They grow simultaneously and symmetrically to both sides of the initial forward crack.
4. The inclined sideways cracks grow at a decreasing load and thus are unstable under load control, They propagate dynamically as soon as the full FPZ forms at the tip of the initial transverse crack or notch. Two-sided propagation is unstable under load control, and thus they can propagate to only one side of the initial transverse crack.
5. Like the forward crack, the sideways cracks, whether inclined or orthogonal, follow Bažant's quasibrittle energetic size effect law. The size effect is stronger in sideways propagation than in the forward growth.
6. The orthogonal sideways cracks (in UD, sCP) can propagate from the initial notch or crack tip only if the sideways-to-forward ratio of fracture energies, Γ_s/Γ_f, is small enough, about 10^{-1} by order of magnitude for orthogonal fracture propagation. Ratio Γ_s/Γ_f increases with decreasing inclination of fibers (or sideways crack) from the initial crack.
7. The sideways fracture energy Γ_s and the corresponding fracture process zone (FPZ) size (or material characteristic length) can be identified from size effect tests with sideways crack growth, as an extension of the size effect method for test-

ing the fracture energy and FPZ size of concrete and other quasibrittle materials.

8. The load required to run the sideways crack decreases with the length of the initial transverse crack or notch. But that length cannot be shorter than the FPZ length.
9. The slopes k of the "stress diffusion lines" bounded by the approximate "stress relief zones" can be effectively calibrated by the J-integral computed by finite elements. Slope k depends on structure geometry and material properties.
10. The foregoing conclusions are verified by the finite element crack band model. Suppressing the spurious mesh sensitivity and ill-conditioning of strain softening, this model captures the effect of both the length and width of the fracture process zone.
11. After a recent demonstration of the existence of gradual postpeak softening in composites and of its agreement with fracture energy (Salviato et al. 2016), the present explanation of sideways crack propagation removes the last argument of some practitioners against the applicability of fracture mechanics and non-statistical size effect to fiber composites.

7 Review of broadly relevant literature

The problem of crack path deflection and branching appears not only for fiber composites but also more broadly for various other materials, whose studies are partly relevant to the present one. One question that has been studied is the stress-based criterion for crack deflection. The first sideways cracks study, based on the local crack-tip stress fields, belongs to Cook et al. (1964). They proposed a stress criterion for the crack deflection into a weak plane perpendicular to primary crack. A stress based criterion was later studied in Goree and Gross (1980), Buczek and Herakovich (1985) and Gupta et al. (1992). Explicit solutions of stress fields near a crack tip in unidirectional composite was given by Sih et al. (1965).

Energy-based criteria were also studied. Sih et al. (1975) proposed for fiber composites a criterion of critical strain energy density, in which they used both the homogeneous and discrete anisotropic elasticity models. Cotterell and Rice (1980) considered the stress intensity factors for different kinking crack angles and related them to the fracture energy release rates for various possible crack directions emanating from the primary crack tip. Many authors followed their idea (Ming-Yuan and Hutchinson 1989; Martnez and Gupta 1994; Ming-Che and Erdogan 1983; Thouless et al. 1989).

Ming-Yuan and Hutchinson (1989), He and Hutchinson (1989), proposed for crack kinking out of a bimaterial interface the criterion $\mathcal{G}_s/\Gamma_s' > \mathcal{G}_f/\Gamma_f$. For the case of an interface between two identical materials they proposed reducing the kinked energy release rate in the criterion to 25% of the energy for forward propagation. He and Hutchinson's energetic criterion for crack kinking was extended to homogeneous anisotropic elastic solids by Suo et al. (1991). Suo et al. rescaled the elastic compliance properties of unidirectional composite for plane strain (or plane stress) using the nondimensional elastic parameters $\lambda = E_2/E_1$ and, $\rho = (E_1E_2)^{0.5}/(2G_{12}) - (\nu_{12}\nu_{21})^{0.5}$. where subscripts 1 and 2 refer to the principal directions of material orthotropy. Considering a pure remote mode I loading and sideways and forward propagation options, Suo et al. proposed, approximately, $0.26\lambda^{-1/4}$ as the critical ratio of the energy release rates. On the other hand, Nairn (1988b), using the "shear-lag" model (Hedgepeth 1961), estimated this ratio as $0.5(G_{12}/E_1)^{1/2}$. A more recent and accurate work for the finite solid geometries was implemented by Xie et al. (2005).

Parmigiani and Thouless (2006) formulated a cohesive zone model combining the strength-based and energy-based criteria, in which cohesive zones of various kinking directions are assumed to co-exist. The kinked direction depended on both the fracture toughness and cohesive strength of various potential directions.

Acknowledgements Partial funding under ARO Grant W911NF-19-1-0039 to Northwestern University is gratefully acknowledged. The first author thanks The Scientific and Technological Research Council of Turkey for financially supporting his post-doctoral research at Northwestern University

References

Andersons J, Tarasovs S, Sparnins E (2010) Finite fracture mechanics analysis of crack onset at a stress concentration in a UD glass/epoxy composite in off-axis tension. Compos Sci Technol 70(9):1380–1385. https://doi.org/10.1016/j.compscitech.2010.04.017

Barenblatt GI (1962) The mathematical theory of equilibrium cracks in brittle fracture. In: Dryden H, von Krmn T, Kuerti

G et al (eds) Advances in applied mechanics, vol 7. Elsevier, Amsterdam, pp 55–129

Bažant ZP (1968) Effect of folding of reinforcing fibers on the elastic moduli and strength of composite materials. Mekhanika Polimerov ; 4: 314–321. Engl. translation in Polymer Mechanics, UDC 678.5.06–419.8+539.3/4

Bažant ZP (1982) Crack band model for fracture of geomaterials. In: Eisenstein Z (ed) Proceedings of the 4th international conference methods geomechanics, held at University of Alberta, Edmonton; vol. 3, pp 1137–1152

Bažant ZP (1984) Size effect in blunt fracture: concrete, rock, metal. J Eng Mech 110(4):518–535. https://doi.org/10.1061/(ASCE)0733-9399

Bažant ZP (1997) Scaling of quasibrittle fracture: asymptotic analysis. Int J Fract 83(1):19–40

Bažant ZP (2005) Scaling of structural strength. Elsevier, Butterworth-Heinemann

Bažant ZP (2019) Design of quasibrittle materials and structures to optimize strength and scaling at probability tail: an apercu. Proc R Soc A Math Phys Eng Sci 475(2224):20180617. https://doi.org/10.1098/rspa.2018.0617

Bažant ZP, Cedolin L (2010) Stability of structures: elastic, inelastic, fracture and damage theories, Oxford University Press, New York, 1991, 3rd edn. World Scientific Publishing, Singapore

Bažant ZP, Kazemi MT (1990) Determination of fracture energy, process zone length and brittleness number from size effect, with application to rock and conerete. Int J Fract 44(2):111–131. https://doi.org/10.1007/BF00047063

Bažant ZP, Le JL (2017) Probabilistic mechanics of quasibrittle structures: strength, lifetime, and size effect. Cambridge University Press, Cambridge

Bažant ZP, Oh BH (1983) Crack band theory for fracture of concrete. Matériaux et Constr 16(3):155–177. https://doi.org/10.1007/BF02486267

Bažant ZP, Planas J (1997) Fracture and size effect in concrete and other quasibrittle materials. CRC Press, London

Bažant ZP, Yu Q (2011) Size effect testing of cohesive fracture parameters and non-uniqueness of work-of-fracture method. ASCE J Eng Mech 137(8):580–588

Bažant ZP, Daniel IM, Li Z (1996) Size effect and fracture characteristics of composite laminates. J Eng Mater Technol 118(3):317–324

Buczek MB, Herakovich CT (1985) A normal stress criterion for crack extension direction in orthotropic composite materials. J Compos Mater 19(6):544–553. https://doi.org/10.1177/002199838501900606

Christensen RM, Lo KH (1979) Solutions for effective shear properties in three phase sphere and cylinder models. J Mech Phys Solids 27(4):315–330

Cook J, Gordon JE, Evans CC et al (1964) A mechanism for the control of crack propagation in all-brittle systems. Proc R Soc Lond Ser A Math Phys Sci 282(1391):508–520. https://doi.org/10.1098/rspa.1964.0248

Cotterell B, Rice JR (1980) Slightly curved or kinked cracks. Int J Fract 16(2):155–169. https://doi.org/10.1007/BF00012619

Cusatis G, Schauffert EA (2009) Cohesive crack analysis of size effect. Eng Fract Mech 76(14):2163–2173

Goree JG, Gross RS (1980) Analysis of a unidirectional composite containing broken fibers and matrix damage. Eng Fract Mech 13(3):563–578. https://doi.org/10.1016/0013-7944(80)90086-7

Gupta V, Argon AS, Suo Z (1992) Crack deflection at an interface between two orthotopic media. J Appl Mech 59(2S):S79–S87

Hashin Z (1965) On elastic behaviour of fiber reinforced materials of arbitrary transverse phase geometry. J Mech Phys Solids 13(3):119–134

Hashin Z (1980) Failure criteria for unidirectional fiber composites. J Appl Mech 47(2):329–334. https://doi.org/10.1115/1.3153664

He MY, Hutchinson JW (1989) Kinking of a crack out of an interface. J Appl Mech 56(2):270–278. https://doi.org/10.1115/1.3176078

Hedgepeth JM (1961) Stress concentrations in filamentary structures. Technical Report NASA-TN-D-882, L-1502, NASA Langley Research Center

Hill R (1965) Theory of mechanical properties of fiber-strengthened materials, III. Self-consistent model. J Mech Phys Solids 13(4):189–198

Hillerborg A, Modeer M, Petersson PE (1976) Analysis of crack formation and crack growth in concrete by means of fracture mechanics and finite elements. Cement Concr Res 6(6):773–781. https://doi.org/10.1016/0008-8846(76)90007-7

Huang Z, Strength Zhou Y (2011) Strength of fibrous composites. Advanced topics in science and technology in China 2011. Zhejiang University Press and Springer, Berlin

Lee S, Pharr M (2019) Sideways and stable crack propagation in a silicone elastomer. Proc Natl Acad Sci 116(19):9251–9256. https://doi.org/10.1073/pnas.1820424116

Martnez D, Gupta V (1994) Energy criterion for crack deflection at an interface between two orthotropic media. J Mech Phys Solids 42(8):1247–1271. https://doi.org/10.1016/0022-5096(94)90034-5

Matzenmiller A, Lubliner J, Taylor RL (1995) A constitutive model for anisotropic damage in fiber-composites. Mech Mater 20(2):125–152

Ming-Che L, Erdogan F (1983) Stress intensity factors in two bonded elastic layers containing cracks perpendicular to and on the interface- I. Analysis. Eng Fract Mech 18(3):491–506. https://doi.org/10.1016/0013-7944(83)90045-0

Ming-Yuan H, Hutchinson JW (1989) Crack deflection at an interface between dissimilar elastic materials. Int J Solids Struct 25(9):1053–1067. https://doi.org/10.1016/0020-7683(89)90021-8

Nairn JA (1988a) Fracture mechanics of unidirectional composites using the shear-lag model II: experiment. J Compos Mater 22(6):589–600. https://doi.org/10.1177/002199838802200605

Nairn JA (1988b) Fracture mechanics of unidirectional composites using the shear-lag model I: Theory. J Compos Mater 22(6):561–588. https://doi.org/10.1177/002199838802200604

Newaz GM (1985) On interfacial failure in notched unidirectional glass/epoxy composites. J Compos Mater 19(3):276–286. https://doi.org/10.1177/002199838501900306

Noselli G, Deshpande VS, Fleck NA (2013) An analysis of competing toughening mechanisms in layered and particulate solids. Int J Fract 183(2):241–258. https://doi.org/10.1007/s10704-013-9890-8

Parmigiani J, Thouless M (2006) The roles of toughness and cohesive strength on crack deflection at interfaces. J Mech Phys Solids 54(2):266–287. https://doi.org/10.1016/j.jmps.2005.09.002

Pineda EJ, Waas AM (2013) Numerical implementation of a multiple-ISV thermodynamically-based work potential theory for modeling progressive damage and failure in fiber-reinforced laminates. Int J Fract 182(1):93–122

Rasoolinejad M, Bažant ZP (2019) Size effect of squat shear walls extrapolated by microplane model M7. ACI Struct J 116(3):75–84

Salviato M, Chau VT, Li W et al (2016) Direct testing of gradual postpeak softening of fracture specimens of fiber composites stabilized by enhanced grip stiffness and mass. J Appl Mech 83(11). https://doi.org/10.1115/1.4034312

Sih GC, Paris PC, Irwin GR (1965) On cracks in rectilinearly anisotropic bodies. Int J Fract Mech 1(3):189–203. https://doi.org/10.1007/BF00186854

Sih GC, Chen EP, Huang SL et al (1975) Material characterization on the fracture of filament-reinforced composites. J Compos Mater 9(2):167–186

Suo Z, Bao G, Fan B et al (1991) Orthotropy rescaling and implications for fracture in composites. Int J Solids Struct 28(2):235–248. https://doi.org/10.1016/0020-7683(91)90208-W

Tankasala HC, Deshpande VS, Fleck NA (2017) Crack kinking at the tip of a mode I crack in an orthotropic solid. Int J Fract 207(2):181–191. https://doi.org/10.1007/s10704-017-0227-x

Tankasala HC, Deshpande VS, Fleck NA (2018) Notch sensitivity of orthotropic solids: interaction of tensile and shear damage zones. Int J Fract 212(2):123–142. https://doi.org/10.1007/s10704-018-0296-5

Thouless MD, Cao HC, Mataga PA (1989) Delamination from surface cracks in composite materials. J Mater Sci 24(4):1406–1412. https://doi.org/10.1007/PL00020229

Xie D, Waas AM, Shahwan KW, Schroeder JA, Boeman RG (2005) Fracture criterion for kinking cracks in a tri-material adhesively bonded joint under mixed mode loading. Eng Fract Mech 72(16):2487–2504

Xu W, Waas AM (2016) Modeling damage growth using the crack band model; effect of different strain measures. Eng Fract Mech 152:126–138

Xu W, Thorsson SI, Waas AM (2015) Experimental and numerical study on cross-ply woven textile composite with notches and cracks. Compos Struct 132:816–824